Bulletin of Faculty of Science, Zagazig University (BFSZU)
e-ISSN: 1110-1555
Volume-2022, Issue-3, pp-75-90
https://bfszu.journals.ekb.eg/journal
Research Paper DOI: 10.21608/bfszu.2022.143974.1148

==========

Delineated and analysis of morphotectonic features utilizing ASTER GDEM/DSM and Radar dataset: An example is Gabel El-Ekma Durba-Arab central Gulf of Suez, Egypt.

Adel M. Seleim [1], Mohamed S. Hammed [2]and Mahmoud H. Bekiet [1]

1 Geology Department, Faculty of Sciences, Al-Azhar University, Nasar City 11751, Cairo, Egypt
2 Geology Department, Faculty of Science, Cairo University, Giza 12613, Egypt

ABSTRACT **: The eastern margin of the central Gulf of Suez comprises the elongate Neoproterozoic basement rocks of Gabel Durba-Araba and Gabel Ekma, which represent sedimentary cover ranging in age from Palaeozoic to Quaternary sediments. Lineaments, a form of geological structure, have risen in popularity recently in geological investigations. It is a widely used structural and geological indicator for establishing general and local tectonic tendencies and fracture zones in rocks, especially in areas covered by basement and sedimentary cover. The global digital elevation/surface model (DEM/DSM) and PLASAR radar data were utilized to distinguish the various structural lineaments' orientation, morphological characteristics, and relationships with distinct tectonic stages exposed in the eastern margin of the central Gulf of Suez comprising the elongate Neoproterozoic basement rocks of Gabel Durba-Araba and Gabel Ekma, which represent sedimentary cover ranging in age from Palaeozoic to Quaternary sediments. Lineaments, a form of geological structure, have risen in popularity recently in geological investigations. It is a widely used structural and geological indicator for establishing general and local tectonic tendencies and fracture zones in rocks, especially in areas covered by basement and sedimentary cover. The global digital elevation/surface model (DEM/DSM) and PLASAR radar data were utilized to distinguish the various structural lineaments' orientation, morphological characteristics, and relationships with distinct tectonic stages exposed in the research region. This data was used for detecting and mapping surface and near-surface structure lineaments. The statical method in the mean of lineament detecting, frequency, length, and density distribution was analyzed using ArcGIS 10.5, PCI Geomatics, and Rockwork 16. Analyze and interpret data related to the different tectonic episodes exposed to the study area. Based on the age of the host basement rift blocks and the overlaying sedimentary cover, we found four population lineament trends. NW and NNE to NE represent the main populations of lineaments affected in the study area. These altered lithological rocks from the Precambrian basement to the Tertiary sediments represent the main structural fault that controls the Gulf of Suez Rift. Other trends represented by WNW and ENE were observed, most probably because of repeated reactivation of tectonism along pre-existing deep structural discontinuities, which are crustal fracture zones. This data was used for detecting and mapping surface and near-surface structure lineaments. The statistical analysis was applied to detect the frequency, length, and density of lineaments using ARC GIS 10.5, PCI Geomatics, and Rockwork 16. Analyze and interpret data related to the different tectonic episodes exposed to the study area. Based on the age of the host basement rift blocks and the overlaying sedimentary cover, we found four population lineament trends. NW and NNE to NE represent the main populations of lineaments affected in the study area. These altered lithological rocks from the Precambrian basement to the Tertiary sediments represent the main structural fault that controls the Gulf of Suez Rift. Other trends represented by WNW and ENE were observed, most probably because of repeated reactivation of tectonism along pre-existing deep structural discontinuities, which are crustal fracture zones.**

KEYWORDS: Gabal Durba-Araba; Central Gulf of Suez; DEM; Shaded relief; Automatic lineaments

---

Date of Submission: 13-06-2022 Date of acceptance: 04-09-2022

I. INTRODUCTION

The Gulf of Suez and the Red Sea represent a modernist continental rift that has been formed because of the severalty of Arabian and African plates (Coleman, 1974; 1993; Hempton, 1987). This separation in the NE direction (Chase, 1978; Jestin et al., 1994; Le Pichon & Francheteau, 1978; McKenzie et al., 1970; Meshref, 2017; Morgan, 2017) led to the opening of the Red Sea between Arabia and Africa, forming a complex structural rift system (Bosworth et al., 1998; Montenat et al., 1988). The exploration geologist has a one-of-a-kind opportunity to study rift-related structural and stratigraphic features (Patton et al., 1994). The geology and tectonics of the Gulf of Suez are largely affected and controlled by the geodynamic processes that have created the Red Sea rift. The Gulf of Suez fault rift system produces areas of superbly exposed outcrop examples of the structures and stratigraphy encountered in the subsurface of the rift basin. The Gulf of Suez Structural patterns have a considerable impact on the studied area's tectonic evolution, which is mostly related to the Red Sea rifting. Structural patterns are characterized by zigzag fault patterns, composed of several prominent structural N-S to NNE-SSW, E-W, and NW-SE striking fault systems, both at the rift borders and within the rift basins (Jarrige et al., 1986; Mostafa, 1993; Mc Clay et al., 1998). The following four tectonic stages affected the Gulf of Suez and developed its structures: The first one is a compressional stage and is oriented NE–SW. This stage is responsible for the reactivation of the N–S to NNE, ENE, and WNW Precambrian fractures. The NW-SE compressional stress regime is related to the WNW, which characterized the second stage of dextral and NNW to N-S sinistral faults. The third stage belongs to the NE–SW extensional regime, which is parallel to the normal NW faults. The NNE–SSW fourth tectonic stage is considered a counterclockwise rotation of the third stage in the Pliocene-Pleistocene age (Zaky, 2017). The first and second stages are considered the initial stages of rifting, while the third and fourth represent the main stages of rifting. The existence of two distinct tectonic stages distinguishes this rifting. Since the early Oligocene, slow subsidence of a continental graben has characterized the first phase (the Red Sea and Gulf of Suez; H. J. Bayer, 1988). Strike-slip motions along the newly constructed Aqaba Dead Sea transform fault system started the second phase (the Red Sea and Gulf of Aqaba), Zaky (2017). Tectonic stages and related structural trends can be categorized as the population of the lineaments and the rock units that cut through them. The eastern central Gulf of Suez area is occupied by igneous and metamorphic rocks of Gabal Durba-Araba, covered by Palaeozoic to Tertiary sediments. The rotated Precambrian basement block of the central Gulf of Suez distinguishes several geologic, tectonic, positive, and negative morphologic features (Fig.1.c). The result of deformation in the area is several geologic structures, such as faults, Oligo-Miocene dykes, and shear zones that have influenced rocks of various geologic ages. These structural discontinuities are often associated with linear geomorphological features such as valleys, ridgelines, and slope breaks that are discernible on the Earth's surface (Jordan & Schott, 2005). Lineament mapping plays a major role in geological studies, especially in mining and petroleum exploration (Marghany & Hashim, 2010). In other words, a detailed geological study imperatively means the knowledge of the present structural information, principally the lineaments (Pour & Hashim, 2015). The latter may correspond to natural objects, including structural alignments (Faure, 2000), geomorphologic consequences (Corgne et al., 2010), structural weaknesses (Masoud & Koike, 2006), faults (Hashim et al., 2013), valleys (Hung et al., 2005; Lacina, 1996), drainage areas, fractures or lines separating the different formations (Hobbs, 1923). Lineaments may also represent the boundaries between the different lithological units of vegetation covers (Abarca, 2006; Marghany & Hashim, 2010; Saadi et al., 2011), or artificial objects (roads, bridges, etc.). In addition, the importance of lineaments is also manifested by their localization, which is often close to several mineralogical deposits (Meshkani et al., 2013; Pour et al., 2016; Pour & Hashim, 2014), which qualifies them as an indirect indicator of mining potential.

Remote sensing data is a vital applied science that has been proven to be highly efficient in the detection, extraction, and mapping of these structural lineaments in a variety of applications. (e.g., Pike, 1991; Hung et al., 2005; Jordan & Schott, 2005; Sarp, 2005; Saadi et al., 2011; Argyriou, 2012; Radaideh et al., 2016a). Identification of lineament structure would be exceedingly difficult if just fieldwork was used. Lineament mapping and analysis is, however, a significant part of neotectonics and structural geology studies since they can provide essential clues about late Quaternary tectonic deformation and environmental hazards (Ali, 2012; Gabrielsen et al., 2002; Jia et al., 2010; Panizza et al., 1987; Ramli et al., 2010; Saadi et al., 2011; Shake & McHone, 1987) Using a suitable software package, lineament extraction from remote sensing data can be done by manual visualization and automatic lineament extraction. The identification lineaments in the automatic technique are more efficient, more accurate, and much faster than in the manual process, which is always influenced by subjective parameters (Das et al., 2018). A major impediment facing automatic extraction is the inability to distinguish geological lineaments from non-geological lineaments, so the resultant maps may contain lineament features derived from other sources besides geological structures, such as railway, power, and fence lines (Leech et al., 2003; Sarp, 2005)

Consequently, automatic approaches have become more popular than those manuals, which are difficult, time-consuming, and highly dependent on the quality of the analysis (Masoud & Koike, 2006). Therefore, remote sensing data has been widely used in lineament mapping (Dubois, 2001; Solomon & Ghebreab, 2006; Masoud & Koike, 2006; Ranganai & Ebinger, 2008; Li, 2010; Corgne et al., 2010; Saadi et al., 2011; Hashim et al., 2013; Meshkani et al., 2013; Pour & Hashim, 2014; Pour & Hashim, 2015; Pour et al., 2016).

The goal of this research is to demonstrate the various tectonic stages that influenced the geographical nature and structural deformation of this area using geospatial data containing limnic length, frequency, orientation, and density. This will give an overview of the tectonic interaction between lineaments and structural characteristics in the studied area. Also, enhancement of the surface structure along the Gabal Durba-Araba and Gabal El Ekma in the central Gulf of Suez using DEM and DSM data Furthermore, detect near-surface lineament structures that are partially masked by loose sediments and difficult to completely recognize in the field or on the optical Landsat images using the potentialities of the DAICHI and the PALSAR radar sensor. Ultimately, the main objectives of this study are the exploration of the minerals and groundwater along the margins of the Gulf of Suez rift based on a good understanding of the genetic and spatial relationships of fracture systems and structural models.

Geologic setting

The continental rift is a narrow, elongated, fault-bound structure in the Earth's crust. The Red Sea is one of the famous fault-bounded rift structures that are often considered the archetypal example of how the continental lithosphere is first rifted and can then evolve into an oceanic spreading system (e.g., Cochran, 1983; Bonatti, 1985; Coleman, 1993; Burke, 1996). The Gulf of Suez formed as the northern segment arm of this rift between the Sinai microplate and the African plate and is widely considered to be currently inactive, but it is important to note that the Gulf of Suez continues to extend at a slow rate today (e.g. (Jackson et al., 1988); Bosworth & Taviani, 1996). It is a prolific extension basin with three asymmetric dip provinces represented by outcrops in the Gabal Durba-Araba area, and Ekma from Neoproterozoic crystalline basement rocks to Quaternary sediments (Fig.1.a &b). The tectonic setting of the area has a complex pattern of geodynamic evolution because its rocks have been influenced by multiple superimposed tectonic regimes, including the two main extensional faults, the rift-bounding fault, and the Rift Coastal fault system of the Durba-Araba fault (Hammed and Sehim, 2002). NNE-SSW is followed by NW-SE, with a secondary trend-oriented E-W fault system forming. The fault system is in the study area, forming hard-linked normal fault segments in zigzag arrays and of two dominant strikes, Gulf parallel NW-trending and Gulf oblique NNE-trending faults (Morley, 1995). The plain area between the two basement blocks is a sedimentary depocenter known as the El Qaa basin (Fig.1a). The Pan-African basement of granitoid, volcanic, sediments, and dikes is exposed in the Durba-Araba fault blocks (Fig.1a). These rocks are grouped into three Late Neoproterozoic rock units, namely, 1) Metavolcanics 2/Granite that is older 3) younger granites (Abdel-Rahman & Martin, 1987). The basement of Gabal Durba-Araba forms two sub-blocks, separated by an NNE-SSW oriented fault (the Durba-Araba Fault), which marks the southern boundary of the Durba block and separates it from the Araba block that lies to the south of them Multiple intrusions of granodioritic to granitic rocks are known as the Older granite (gray) and the Younger granite (pink), which were emplaced during the Precambrian Cratonization of the Arabo-Nubian shield (Patton et al., 1994). The Durba-Araba Fault has an oblique-slip displacement and dips 65° NW (Moustafa, 2004). It shows good evidence of drape folding of the overlying sedimentary section toward the NW as well as good evidence of left-lateral strike-slip displacement. The Paleozoic sedimentary section juxtaposed against the Precambrian basement outcrop on the northern side of the fault has an NW dip of about 25° and indicates drape folding over the NW dipping surface of the fault. This sequence comprises a thick pre-rift section of Paleozoic-lower Cretaceous clastic of Nubia sandstones and upper Cretaceous-Eocene mixed clastic and carbonates that unconformably overlie the Precambrian basement (Abdallah & El-Adindani, 1963). The upper Cretaceous sequence includes sandstones and shales of the Cenomanian Raha Formation; limestone of the Turonian Wata Formation; thick sandstones and shales of the Coniacian-Santonian Formation; and Campanian Maastrichtian Sudr Chalk (Ghorab, 1961; Youssef, 1957). Marine conditions persisted through the Paleocene and Eocene, depositing shales of the Esna Formation and thick Eocene carbonate formations (William Bosworth et al., 2014). Winn, Jr. et al., 2001; Abd El-Motaal, 1993). The Miocene rocks include distal and proximal facies of shallow-marine calcareous sandstones and conglomerates, open-marine marls, reefal carbonates, and interbedded evaporites and shales. They are classified here as Nukhul, Rudeis-Kareem, and Belayim-South Gharib-Zeit formations (Darwish & El Azaby, 1993; Hammed, 2002). The Pliocene to Quaternary deposits includes alluvial fans, beach deposits, coastal fan deltas, and wind-blown sands on the wadi floors.

II. MATERIALS AND METHODS

The main objectives of the methodology adopted in this study aimed to achieve detection and mapping of geological structures like faults and lineaments automatically occurring within the area by using two types of

data: ASTER (DEM/DSM) and radar satellite datasets. The radar data includes phased array type L-band synthetic aperture radar (PALSAR) acquired from Japan Resources Observation System Organization (JAROS), i.e., horizontal transmit-horizontal receive (HH) polarization for JERS-1 data; HH and horizontal transmit-vertical receive (HV) polarization for ALOS-2/PALSAR-2 data. The longer wavelength L-band SAR data (23.5 cm) can penetrate the surface to a few meters' depth in very dry soils with low electrical losses and can image the near-surface structures (Owe & de Griend, 1998; Barrett et al., 2009; Paillou, 2017) The penetrated depths and the intensity of returned backscattered energy are very sensitive and dependent on two main types of parameters (Leech et al., 2003); (1) sensor parameters (wavelength/frequency, polarization, incidence angle, orbit), and (2) ground parameters (topography, surface roughness, object geometry, and orientation, dielectric constant). The sconed data is the Global Digital Elevation/surface model (DEM/DSM) overview and processing status of the ALOS World 3D (AW3D) project. All the preprocessing of this data had already been done by the data provider using their Sigma-SAR processor, which involved radiometric and geometric calibration, ortho-rectification, slope correction, co-registration, and intensity tuning of neighboring strip data (Fig.2).

In this study, lineaments' analytical methods were mapped using hill-shaded images produced from ASTER-(DEM/DSM) and radar (HH &HV) ALOS-2/PALSAR-2 data. In tectonically high deformation areas, analytical hill-shading techniques are commonly utilized to recognize linear structures with specific orientations (e.g., Pike, 1991; Deffontaines et al., 1997; Jordan and Schott, 2004; Jordán et al., 2005; Abarca, 2006; Arrowsmith & Zielke, 2009; Argyriou, 2012; Langridge et al., 2014). The topographic relief of the Earth's surface is shown via analytical hill-shading. It is commonly based on replicating the impact of light originating from a source of illumination with a specified height and azimuth (Batson et al., 1975; Horn, 1981). In a hill-shaded map, objects are either concealed or emphasized depending on the lighting azimuth and tilt. Features parallel to the light beam are often more difficult to identify than those perpendicular to the illumination. (Cooper, 2003; Jordan & Schott, 2005; Abdullah et al., 2010; Das et al., 2018). Accordingly, we apply different sun azimuth values to the hill-shaded map produced from ASTER-(GDEM/DSM) for the research region. A visual analysis of lineaments extracted from a hill-shaded map reveals that some of the linear characteristics recognized at one azimuth angle of the light source are not visible or are only weakly visible at another. A hill-shaded image is produced from varied azimuth angles of the light source to overcome the constraints of the lighting influence on the appearance of linear features (Radaideh et al., 2016). According to the nature of the study area, multi-illumination hill-shaded images with a light azimuth covering a range of 360°, 45°, 90°, and 135° (Easting) and a second multi-illumination hill-shaded covering a range of 180°, 225°, 270°, and 315° (Westing) and a light elevation of 45° were then used for automatic lineament extraction. The purpose of this approach was to guarantee that the lineaments produced by two hill-shaded images with various light azimuth combinations were similar. The combination of several lighting azimuth angles into a single image gives vital insight into the diverse spatial patterns of the linear characteristics that would not be seen if only a single illuminated hill-shaded image was employed (e.g., Mark, 1992; Onorati et al., 1992; Loissios et al., 2021; Abdullah et al., 2009, 2010). Identification of lineaments was also performed on both radar (HH & HV) and ALOS-2/PALSAR-2 data to detect near-surface linemate structure discrimination. In addition, the geological and topographical maps of the Sinai were also used. The techniques were performed using PCI-Geomatica, ESRI ArcGIS 10.5, and Rock Works 16 software.

Lineament Extraction

In this investigation, the lineaments extraction module was run with the PCI-Geomatica v.16 software's default parameters. All three phases of edge detection, thresholding, and curve extraction were completed in three steps (Geomatics, 2015). Six threshold settings were used to extract the linear curvature polyline in the vector layer: (RADI (Filter Radius) = 10; GTHR (Edge Gradient Threshold) = 100; LTHR (Curve Length Threshold) = 30; FTHR (Line Fitting Threshold) = 3; ATHR (Angular Difference Threshold) = 30; and DTHR (Linking Distance Threshold) = 20 (Sarp, 2005; Geomatics, 2015). Vector data map uploaded to Arc Gis 10.5 software as a shapefile. Split line at vertex and calculation geometry informs of Azimuth and length for further interpretation and analysis (Tchoukanski, 2015). Rockwork v.16 generated a frequency-weighted and length rose diagram for each lineament dataset to find the prevailing azimuth frequency of lineation (Fig.2).

III. RESULTS AND DISCUSSION

3.1. Lineament Directional Analysis

Automated lineament mapping was able to capture many intersecting populations of lineaments of varied lengths and orientations using remote sensing datasets. Different multi-illumination hill-shaded images were created from different light azimuths to represent the combination of different light from easting and westing azimuths (Fig 3&5). The study area contains different topographic high and low display surface relief features in different

directions and displays a sequence of positive and negative elements (Fig.1c). The negative relief features mostly represent faults, valleys, trenches, and joints, while positive relief elements represent elevated topography (Radaideh et al., 2016). The directional analysis of automatically extracted lineament maps has been done with references to the fault map of the study area. In addition, a length-frequency distribution diagram, as well as length-weighted and rose diagrams for each lineament population were created (Fig.4 & 6). Accordingly, lineaments were divided into eight azimuth groups or lineament populations: N, NNE, NE, ENE, E, NNW, NW, and WNW. The Rose diagram illustrates the extracted structural lineaments map. The basic statistics for each lineament population are given in Table 1, which summarizes the results of the investigation. Four patterns are identified from the east and wasting light azimuth: NW, NNW, NNE, N-S, and, to a limited extent, NE. On the contrary, structural patterns such as WNW, ENE, and E-W are less common. The same result can be observed from the HH and HV PALSAR lineaments with the smaller number of lineament populations. Simply put, the regional fracture systems driving the tectonics of the central Gulf of Suez are represented by two primary dominating clusters: NW-SE to NNW-SSE and N-S to NNE-SSW.

3.2. Lineament Length Analysis

Analysis of the lineament length is a useful guide for interpreting the lineament map. Lineament lengths were measured using a GIS application and displayed as mean lengths. The mean length was computed, and the resulting values were contoured throughout the study area. Combination and merge of different lineament azimuths have been performed to clear the main structural trend that affects the study area. This may lead to duplicate lineaments. Accordingly, the correction has been performed by Remove identical by Arc Gis software. Figure (9&10) shows that 8408 lineaments have been recognized, ranging in length from 0.0548 to 12.6895 km, with a total length of 5,347.5 km (Table.1). Analysis of the different lineaments trend indicates that the NW-SE lineament (Gulf-parallel trend) has high frequencies of length compared with the other trends. According to the parameter that is used in this study, the maximum length of 8.1 km is recorded by the NW-SE lineaments trend followed by the N-S whereas the NNE-SSW (Aqba-trend) and Gulf- orthogonal E-W to ENE trends have fewer lengths.

3.3. Lineament Density

The density map is widely used in lineament study parameters (Hung et al., 2005; Cologne; Hashim et al., 2013). It can be informed in a variety of ways, including the number of lineaments per unit area (Hashim et al., 2013). In the current work, lineament density was created to find and compare the relationship between the concentration of lineaments and the proration of faults that affect the study area regarding the geological maps (Fig.11). The research region is divided into three basement rift block segments, indicated from south to north by G. Araba, G. Abu Durba, and G. El Ekma.

The concentration of lineaments varies from one segment block to another because of diverse tectonic processes, resulting in the existence of four primary trends directed NW, N–S, E–W, and NE–SW over the whole region. G. Araba represents the southern segments of the study region (Fig.11), which has a strong dominance of NW lineaments. This trend represents the primary structural trend of the Gulf of Suez rift. Following that are the many minor trends (e.g., NE, WNW, and N-S. Fig.6). Further north, at G. Abu Durba, we find the largest concentrations of the lineaments represented by Also, the NW trend is followed by the WNW and N-S trends in that order (Fig.11). G. El Ekma is influenced by a high concentration of different lineament trends, with the NW being the most prevalent, followed by N-S, NE-SW, and finally ENE-WSW (Fig.11).As indicated above, the density map is divided into five main categories: low (0-274 m2/m2); moderate (354-548 m^2/m^2); high (708-823 m^2/ m^2); remarkably high (1097-1371 m^2/ m^2); and extremely high (>1371 m^2/m^2). Most of the studied region has a low to moderate lineament density. The density of lineaments develops in the southern and northern sectors, where values range from high to extremely high (Fig.11). This might be due to the presence of older basement rocks (G, Araba) in the southern part and sedimentary cover in the north (G. El Ekma), which have a great ability to express various fracture systems because of their lithological nature and exposure to various tectonic episodes. On the other hand, the G. Abu Durba at the central portion of the entire area has fewer lineaments than other parts. This refers to the naturality of its youngest lithological rock units.

Tectonic Prominence of Structural Lineaments

In this study, DSM/DEM and PALSAR data were utilized to automate lineament extraction using the default parameters of the PCI-Geomatica algorithms software. A description of the many lineament populations found in various locations throughout the study area will be presented, with an emphasis on the major lineament

populations. According to the age of the host rock and weight rose diagram analysis, the lineaments divided into four populations can be detected in the Precambrian basement, early Paleozoic, Mesozoic, and tertiary rocks. The Quaternary was not studied in this research. Nemours lineaments have a wide range of trend, frequency, length, and density. NW, N-S, NNE-SSW, ENE-WSW, and WNW-ESE are the trends of these features. The NW trend is the most common and longest, affecting Precambrian basement rocks of G. Araba via the linear characteristics of the Arab bonding fault and Oligo-Miocene dikes, while it is strongly represented in the Cretaceous to Miocene strata of G. Qabliat in the east. Also, the Araba basement block is divided into segments because of links between NW and NNW, and N-S. Fault systems create zigzag pattern segments (Moustafa, 2004). G. Araba, as well as a few minor occurrences at G. Qabliat. Most of these faults die out in the Raha Formation, and only one reaches the Sudr Formation (Moustafa, 2004). G. Abu-Durba is the youngest phase of younger granite dissected by the NW lineament feature representing the NW rift bounding fault (Abu Durba fault) and NW Oligo-Miocene dikes, as well as minor trends of NE, ENE, and WNW. G. Abu Durba is separated from G. Araba by an NNE-SSW left-lateral strike-slip fault with oblique-slip displacement and substantial drape folding of the overlying sedimentary strata toward the NW (Moustafa, 2004). To the north of G. Abu Durba, the G. Ekma block represents a sedimentary cover of Eocene and Miocene clastic and evaporite. The block is highly dissected by many normal faults-oriented NW-SE and NNW-SSE, followed by NE, ENE, and WNW lineaments trends. The northern side of the block is bounded by an NNE-SSW-oriented normal fault (Ekma-Nazzazat Fault) that represents a transfer fault between the Nazzazat and Ekma Faults (Moustafa & El-Raey, 1993; Moustafa, 2004). The tectonic style of the principal structural extracted lineaments of the area under investigation refers to the complex pattern and the movements recorded by the various fault trends during the Miocene. These faults were generated by repeated reactivation of pre-existing crustal fractures and old faults during the Oligo-Miocene rift stage. The structure that is created accordingly cannot be the result of a simple extension inducing the creation of neo-formed faults (Ott et al., 1998). Thus, the Gulf of Suez and the Red Sea rift are not a pure neo-formed Cenozoic structures but recombination and reactivation of pre-existing discontinuities during the Tertiary.

V –CONCLUION

The results of the combined use of remote sensing and GIS analytic methods to explain the intricate and complicated patterns of late Precambrian to Quaternary lineament features in the central Gulf of Suez are presented in this study. Hill-shaded images derived from a global digital elevation/surface model (DEM/DSM) and L-band SAR horizontal receive (HH) polarization for JERS-1 data; and HH and horizontal transmit-vertical receive (HV) polarization for ALOS-2/PALSAR-2 data with varying spatial resolutions were used to automatically extract linear features and analyze their tectonic significance in the study area. The application of multi-illuminated hill-shading procedures allowed us to resolve impediments in the determination of linear surface and near-surface features, which would be unresolvable if only one lighted hill-shading image was used. The length of the lineament used to evaluate the lineament map demonstrates that the NW-SE lineament (gulf-parallel trend) has higher length frequencies than the other trends. According to the parameters employed in this study, the NW-SE lineman trend has the longest length of 8.1 km, followed by the NNE-SSW (Aqaba trend) and gulf-orthogonal E-W to ENE, while the WNW-ESE trends have shorter lengths. The directional analysis of the automatically derived lineaments map was performed regarding the study area's geological map. The results confirm the similarities in the directional behavior of the lineaments, fault lines, and structures. The overall map of the principal lineaments representing all the distinct segments indicates four trends in lineament orientation: NW-SE, NNE-SSW, WNW-ESE, and E-W, with the first direction predominating. This conclusion accords with the NW-SE compression impact of the Oligo-Miocene main tectonic phase responsible for the NW-SE Clysmic faults' implementation. Other trends are related to the repeated reactivation of pre-existing crustal structures during various tectonic episodes. All these Neoproterozoic lineaments were reactivated by the Late Oligocene-Miocene GOS extension as Gulf-parallel NW-trending faults linked with ENE-Gulf-orthogonal and NNE-gulf-oblique transfer faults. The Gulf-parallel lineaments are acted as normal faults and are presented by the Rift Bounding fault to the west of Gabal Durba-Araba and Ekma where the Precambrian basement rocks of G. Araba, Abu Durba, and El Ekma are exposed in the western part of the study area and bounded by an NW-SE oriented fault. The Gulf-oblique lineaments are mainly acting as transfer faults as the northern separation between G. Durba and G. Araba shows left-lateral shearing sense as manifested by the NE-Aqaba trending fault of the Wadi Araba strike-slip fault crossing the G. Durba-Araba range to the east and its show evidence includes 1) offset between the Durba and Araba blocks 2) offset of some NW-SE oriented dikes on both sides of the fault. El Ekma fault linked to the NNE-SSW oriented transfer fault on the northern side of the Durba block represents a right lateral Strick slip fault. The Gulf-orthogonal lineaments also acted as transfer faults in the massive basement to the east of the study area.

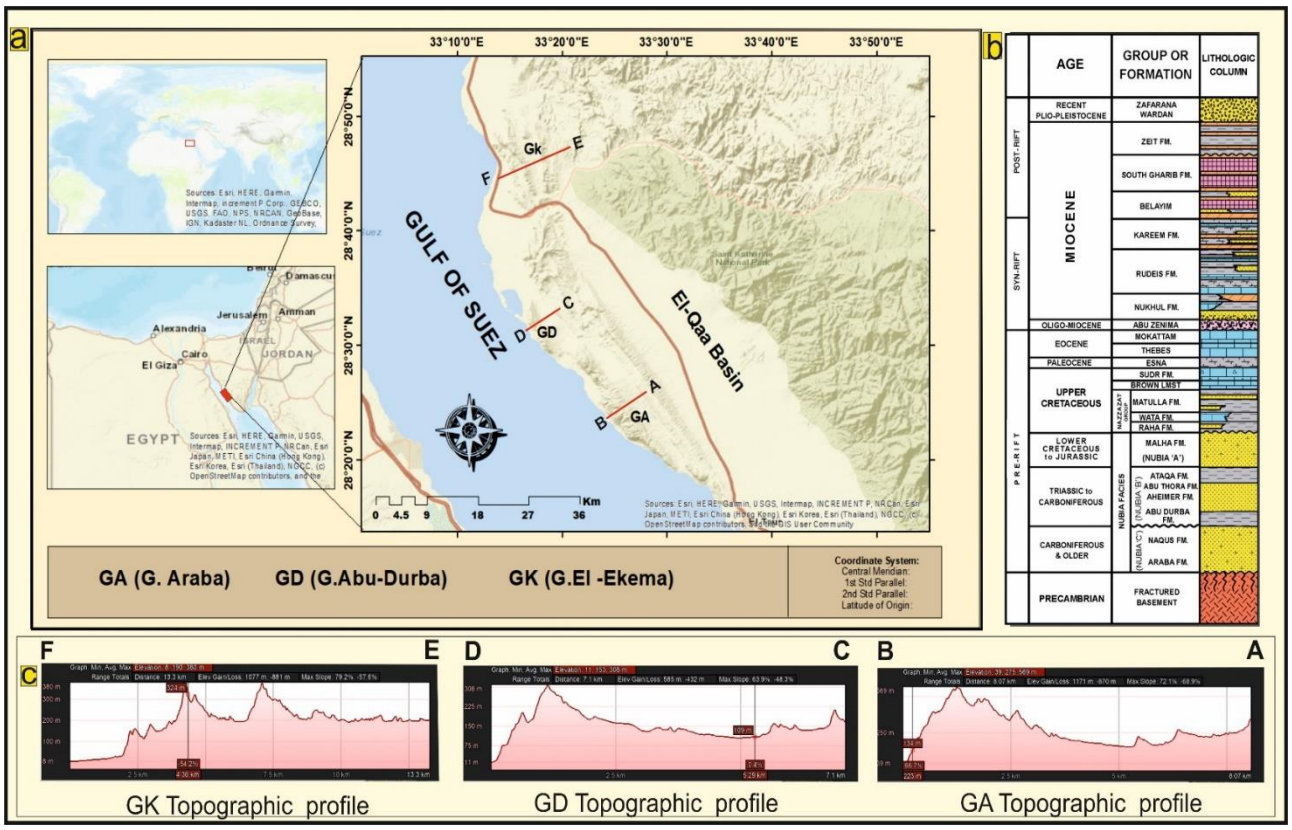

Fig.1. a Topographic map concerning Egypt map showing the locations of the study area. (b) Generalized stratigraphic Colum of Gulf of Suez, Egypt (EGPC, 1996)., (c) Vertical topographic change in surface elevation, as well as transects A–B, C–D, and E–F, show distinct positive and negative relief

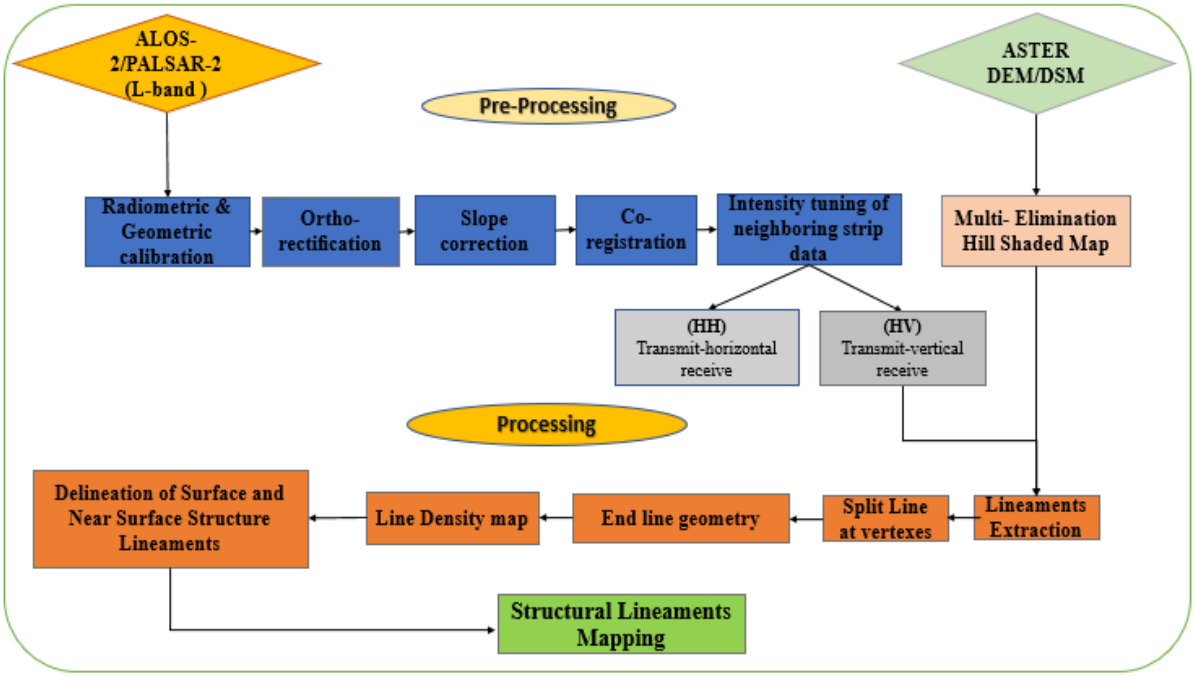

Fig.2. Methodological flowchart showing the procedure used in this study and its characteristics of the image processing and analysis algorithm

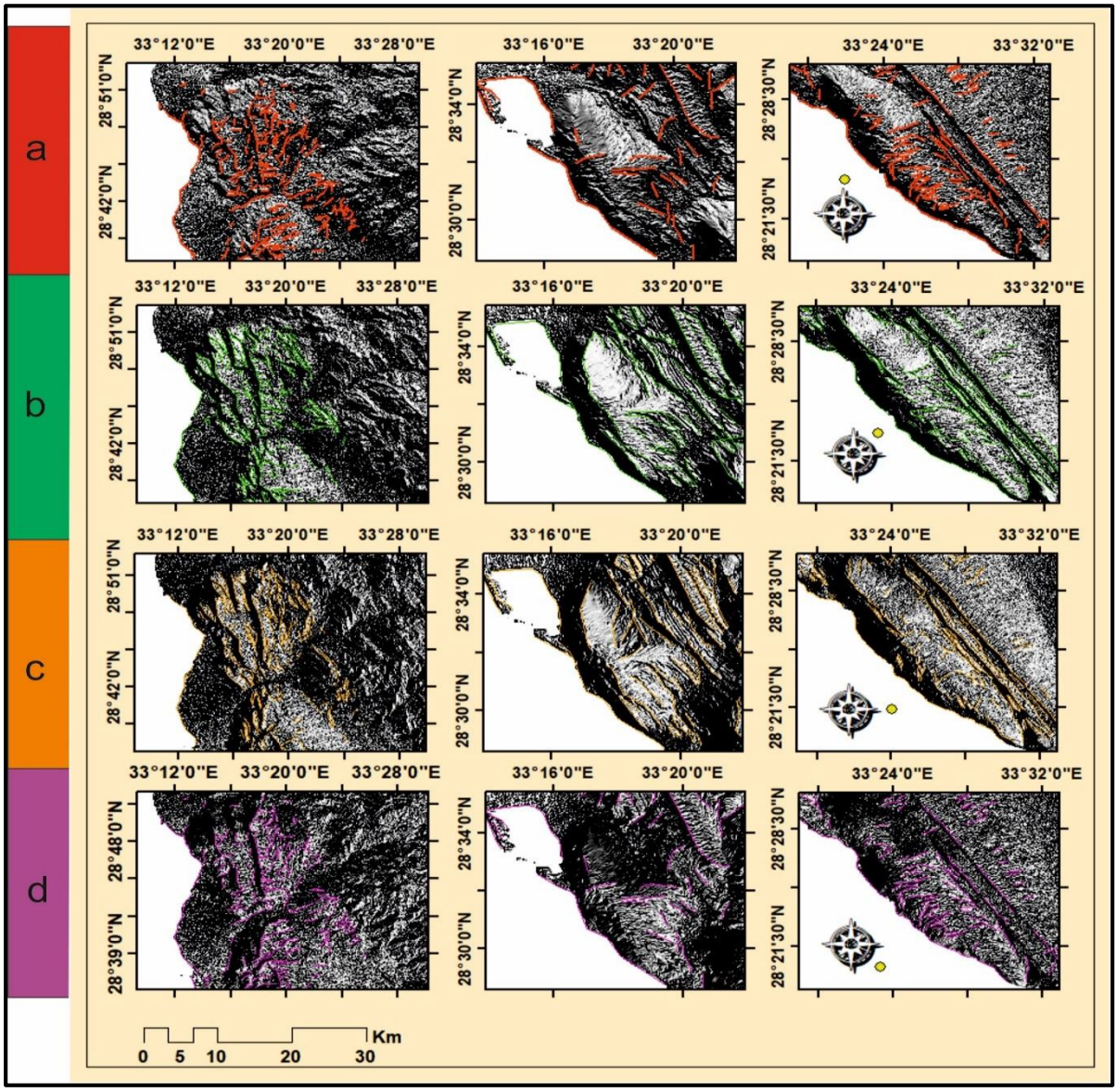

Fig.3. lineament map generated by the combination of lineaments automatically derived from ASTER GDEM/DSM, a multi-illumination hill-shaded image with the light source azimuth of **a.** 360°, **b.** 45°, **c** 90°, and **d.** 135°.

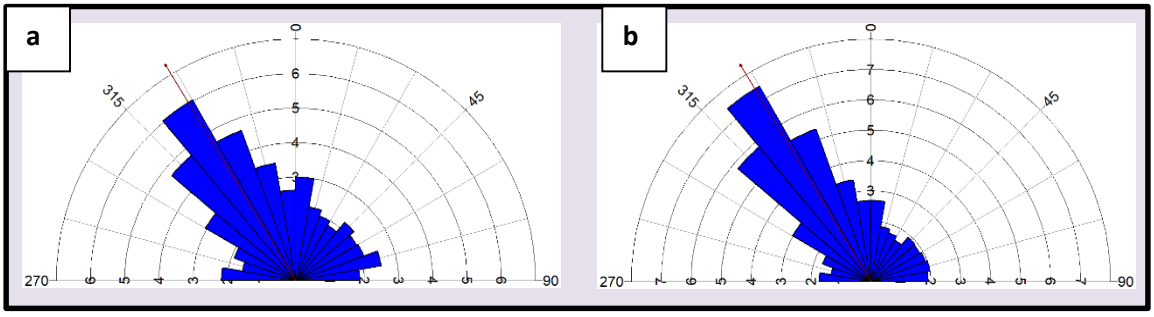

Fig.4 The dominating azimuth orientations for each lineament population with the light source azimuth of 360°, 45°, 90°, and 135°.are depicted using **a**. frequency and **b**. length weighted rose diagrams. **.**

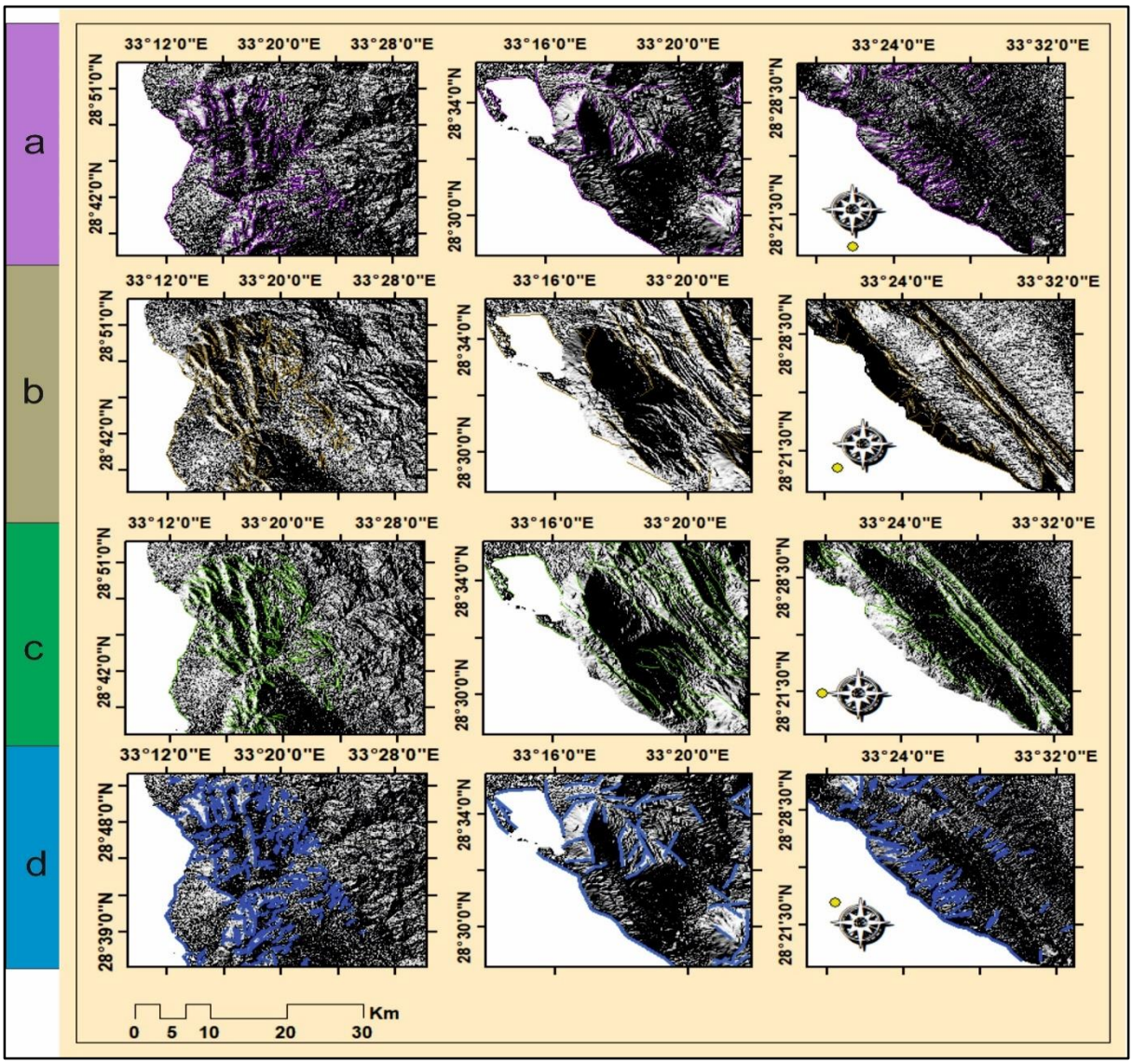

Fig.5. lineament map generated by the combination of lineaments automatically derived from ASTER GDEM/DSM, a multi-illumination hill-shaded image of G.ElEkma with the light source azimuth of a. 180° , b. 225°, c.270° and d 315°.

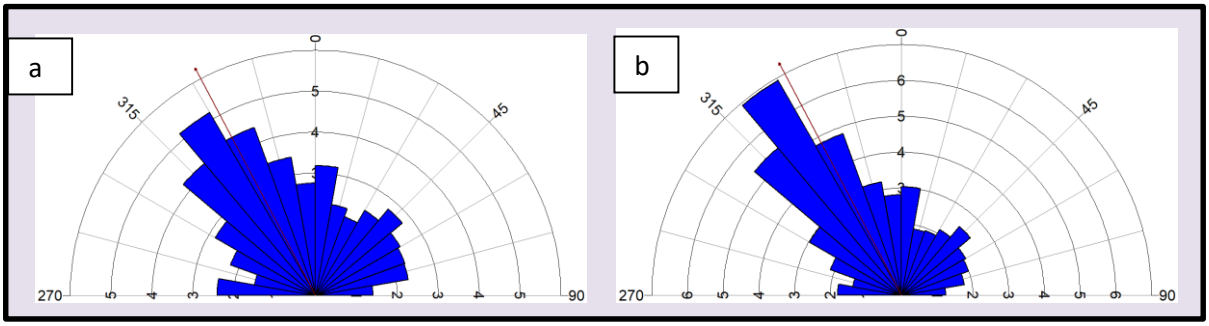

Fig.6 The dominating azimuth orientations for each lineament population with the light source azimuth of 180°, 225°, and 270° are depicted using a. frequency and b. length weighted rose diagrams.

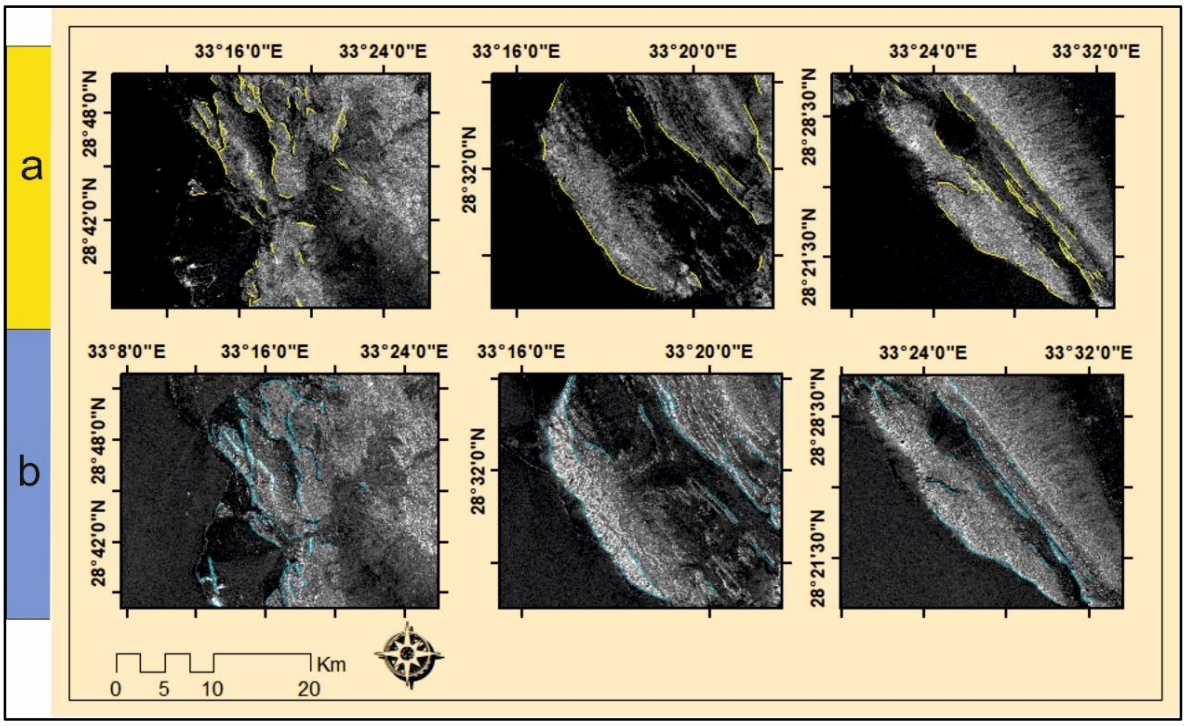

FIG.7. LINEAMENT MAP AUTOMATICALLY DERIVED FROM ALOS/PALSAR A. HV AND B. HH TRANSMIT RECEIVE DETECT THE NEAR SURFACE STRUCTURAL LINEAMENTS

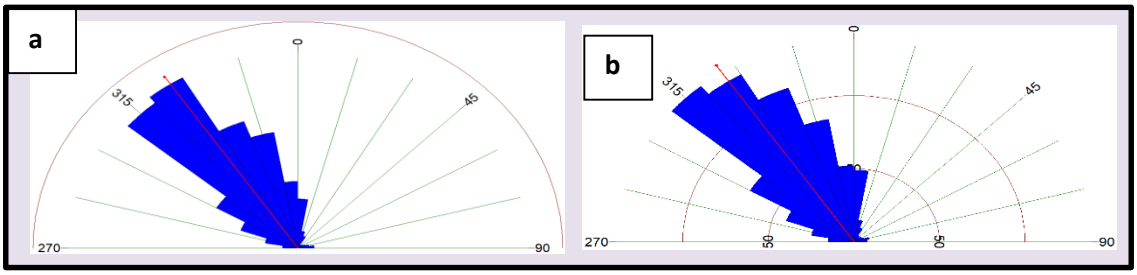

Fig.8. The dominating azimuth orientations for lineament population of HH &HV are using a. frequency and b. length weighted rose diagrams

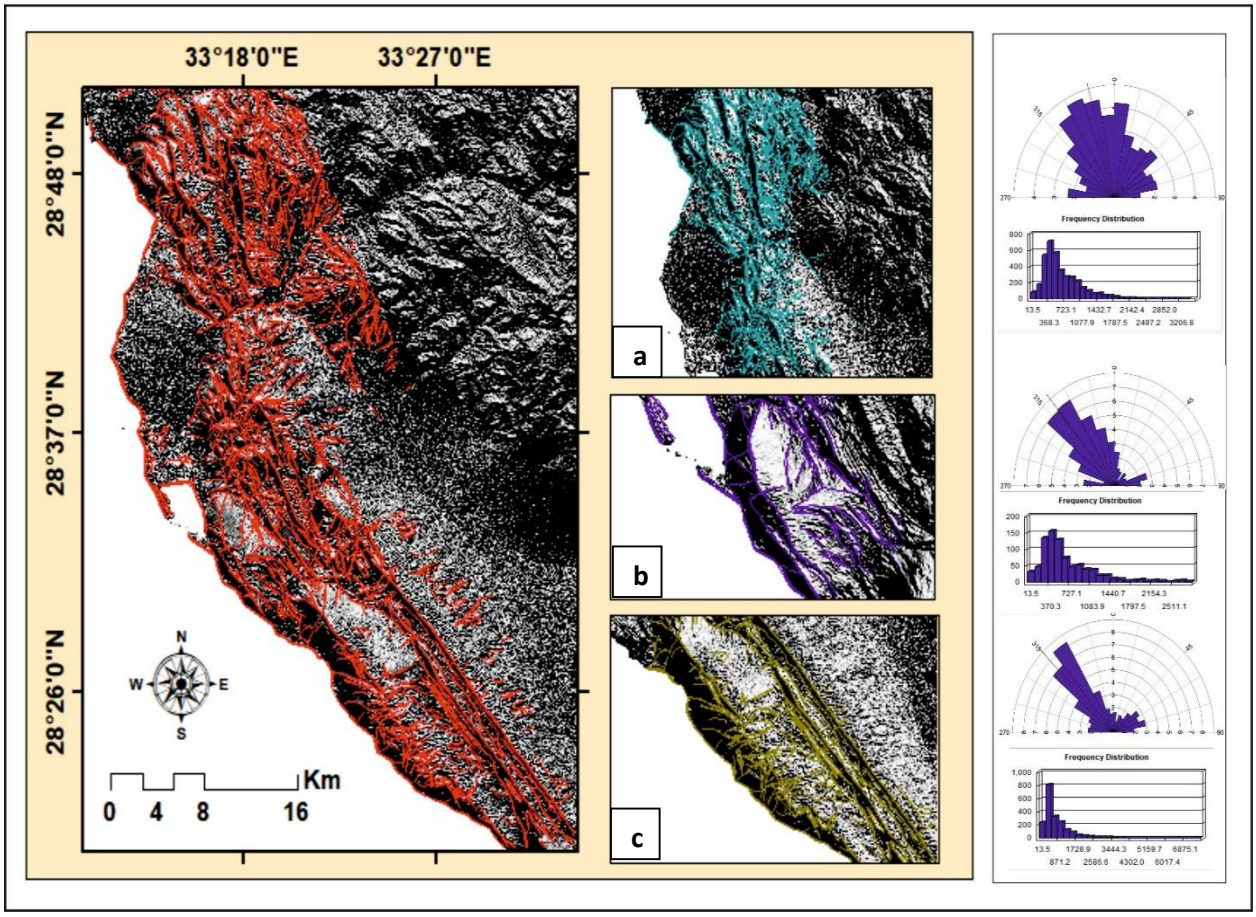

FIG.9. FINAL LINEAMENT MAP CREATED BY THE COMBINATION OF EASTING AND WESTING LIGHT SOURCE AZIMUTH AUTOMATICALLY DERIVED FROM ASTER GDEM/DSM CLEAR SEVERAL INTERSECTING SETS WITH MULTI LENGTH AND DIFFERENT ORIENTATIONS OF A. G. EL-EKMA B. G. ABU DURBA AND C. G. ARABA.

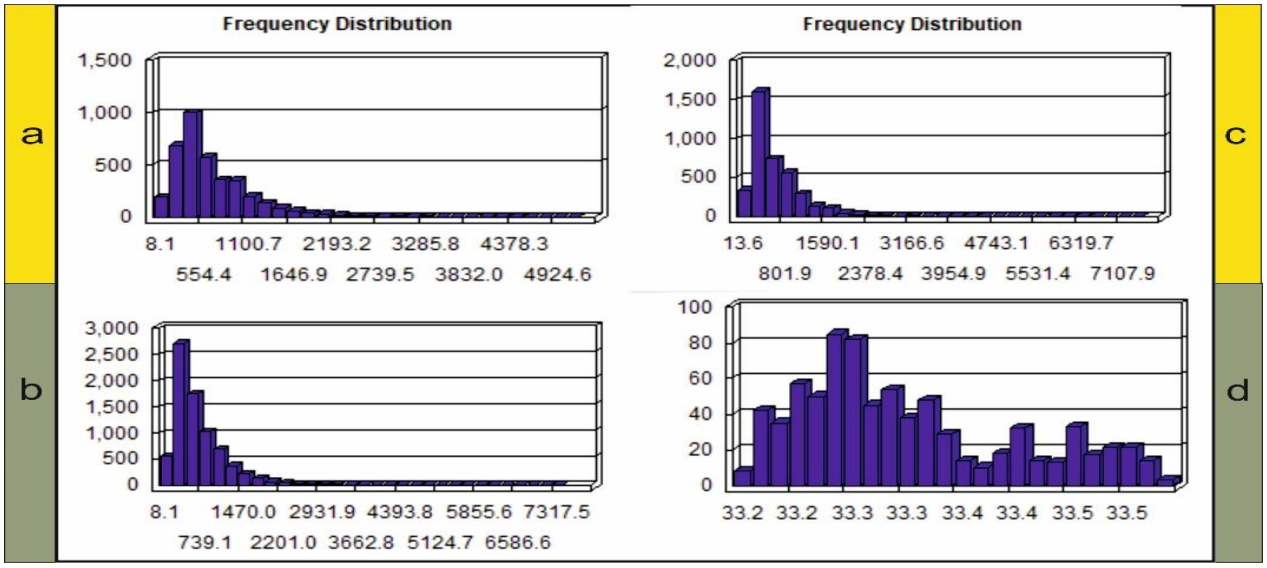

Fig .10. Distribution histograms showing the Statistic of lineaments regarding to the length for the (a) Easting (b) Westing azimuth, (c) All lineament combination azimuth (d) HH &HV images.

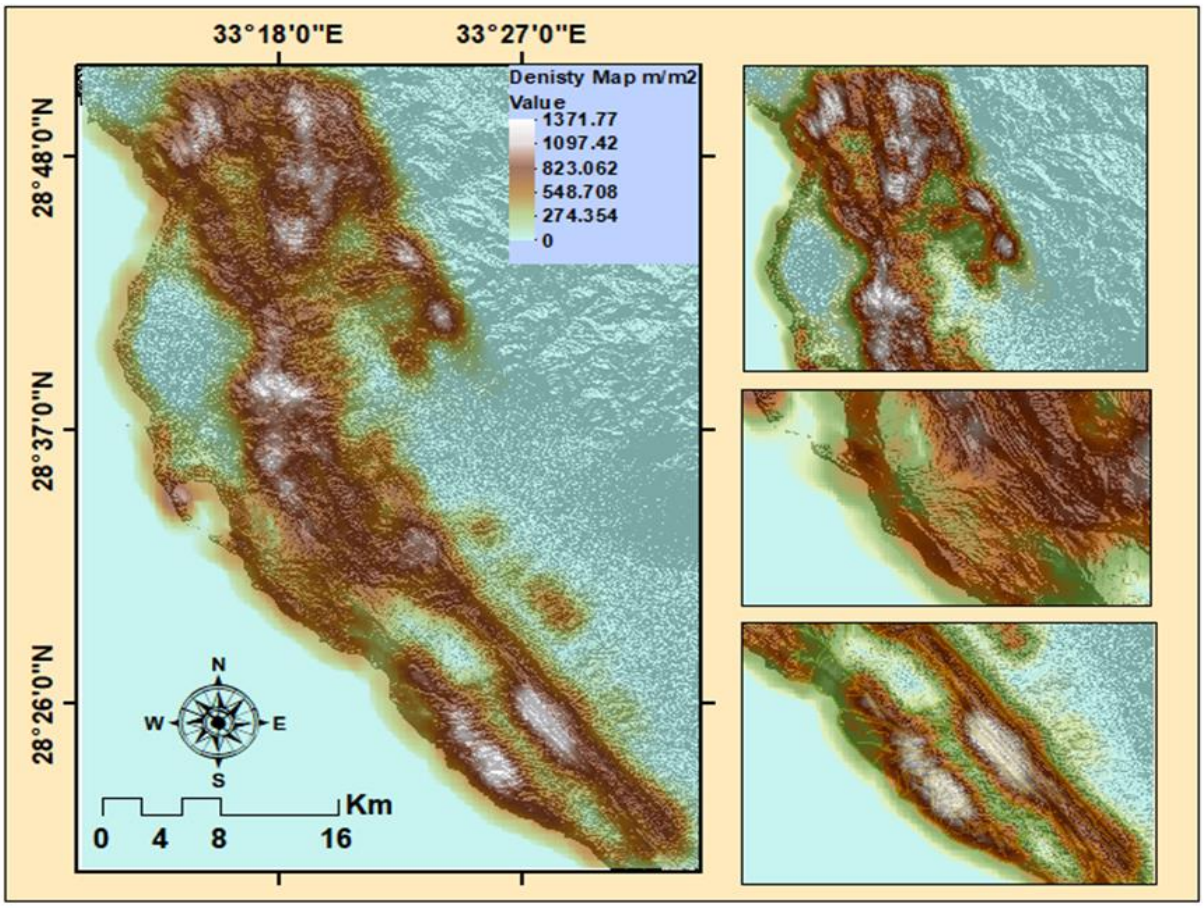

Fig. 11. Lineament density map clear zones of maximum lineament density anomalies probably indicate a higher intensity of deformation. The G. Abu Durba at the central- portion of the entire area has fewer lineaments than other parts. this refers to the naturality of its youngest lithological rock units (Phase III younger granite) and therefore the lack of tectonic phases to which it was exposed

Table.1. Statistical summary of the automatic lineament maps extracted from multi-illumination hill-shaded images and ALOS/PALSAR data.

Map	Multi-illumination hill-shaded images		PALSAR	ALL DATA
Character	(0°, 45°, 90°, and 135°)	(180°, 225°, 270°, and 315°)	(HV)&(HH)	COMBINATION
No of. lineaments	3755	3870	783	8408
Min. length (m)	8.1397	13.595	33.2	54.8
Max. length (m)	5169	7487	33.5	12689.5
Total length (km)	2,629.7	2,691.7	26.1	5,347.5

REFERENCES

Abarca, M. A. A. (2006). LINEAMENT EXTRACTION FROM DIGITAL TERRAIN MODELS.

Abd El-Motaal, E. (1993). Structural studies on the sedimentary rocks in the Red Sea coastal plain between lat. 25 45′ and 26 00′ N., Egypt. Ph. D. Thesis, Geology Dept., Faculty of Science, Al-Azhar University.

Abdallah, A. M., & El-Adindani, A. (1963). Notes on the Cenomanian--Turonian contact in the Galala Plateau,

Eastern Desert, Egypt. Egyptian Journal of Geology, United Arab Republic, 7(1), 67–70.
Abdel-Rahman, A.-F. M., & Martin, R. F. (1987). Late Pan-African magmatism and crustal development in northeastern Egypt. Geological Journal, 22(4), 281–301.
Abdullah, A., Akhir, J. M., & Abdullah, I. (2009). A comparison of Landsat TM and Spot data for lineament mapping in Hulu Lepar Area, Pahang, Malaysia. European Journal of Scientific Research, 34(3), 406–415.
Abdullah, A., Akhir, J. M., & Abdullah, I. (2010). Automatic mapping of lineaments using shaded relief images derived from digital elevation model (DEMs) in the Maran-Sungi Lembing area, Malaysia. Electronic Journal of Geotechnical Engineering, 15(6), 949–958.
Ali, M. (2012). Identifying Neotectonic Features Using Lineament Analysis of Satellite Images in Tectonically Active Muzaffarabad Area. Azad Jammu \& Kashmir (M. Sc. Thesis) National Centre of Excellence in Geology (NCEG), University of Peshawar, Peshawar, Pakistan.
Argyriou, A. (2012). A methodology for the rapid identification of neotectonic features using geographical information systems and remote sensing: A case study from Western Crete, Greece. University of Portsmouth Greece.
Arrowsmith, J. R., & Zielke, O. (2009). Tectonic geomorphology of the San Andreas Fault zone from high resolution topography: An example from the Cholame segment. Geomorphology, 113(1–2), 70–81.
Barrett, B. W., Dwyer, E., & Whelan, P. (2009). Soil moisture retrieval from active spaceborne microwave observations: An evaluation of current techniques. Remote Sensing, 1(3), 210–242.
Batson, R. M., Edwards, K., & Eliason, E. M. (1975). Computer-generated shaded-relief images. Journal of Research US Geol. Survey, 3(4), 401–408.
Bonatti, E. (1985). Punctiform initiation of seafloor spreading in the Red Sea during transition from a continental to an oceanic rift. Nature, 316(6023), 33–37.
Bosworth, William, Khalil, S., Clare, A., Comisky, J., Abdelal, H., Reed, T., & Kokkoros, G. (2014). Integration of outcrop and subsurface data during the development of a naturally fractured Eocene carbonate reservoir at the East Ras Budran concession, Gulf of Suez, Egypt. Geological Society, London, Special Publications, 374(1), 333–360.
Bosworth, William, & Taviani, M. (1996). Late Quaternary reorientation of stress field and extension direction in the southern Gulf of Suez, Egypt: Evidence from uplifted coral terraces, mesoscopic fault arrays, and borehole breakouts. Tectonics, 15(4), 791–802.
Bosworth, WPRJB, Crevello, P., Winn, R. D., & Steinmetz, J. (1998). Structure, sedimentation, and basin dynamics during rifting of the Gulf of Suez and north-western Red Sea. In Sedimentation and tectonics in rift basins red sea:-Gulf of Aden (pp. 77–96). Springer.
Burke, K. (1996). The african plate. South African Journal of Geology, 99(4), 341–409.
Chase, C. G. (1978). Plate kinematics: The Americas, East Africa, and the rest of the world. Earth and Planetary Science Letters, 37(3), 355–368.
Cochran, J. R. (1983). A model for development of Red Sea. Aapg Bulletin, 67(1), 41–69.
Coleman, R. G. (1993). Geological evolution of the Red Sea. Oxford Monographs on Geology and Geophysics. Oxford University Press, New York, 186.
Cooper, G. R. J. (2003). Feature detection using sun shading. Computers \& Geosciences, 29(8), 941–948.
Corgne, S., Magagi, R., Yergeau, M., & Sylla, D. (2010). An integrated approach to hydro-geological lineament mapping of a semi-arid region of West Africa using Radarsat-1 and GIS. Remote Sensing of Environment, 114(9), 1863–1875.
Darwish, M., & El Azaby, M. (1993). Contributions to Miocene sequences along the western coast of the Gulf of Suez, Egypt. Egyptian Journal of Geology, 37, 21–47.
Das, S., Pardeshi, S. D., Kulkarni, P. P., & Doke, A. (2018). Extraction of lineaments from different azimuth angles using geospatial techniques: a case study of Pravara basin, Maharashtra, India. Arabian Journal of Geosciences, 11(8), 1–13.
Deffontaines, B., Lacombe, O., Angelier, J., Chu, H. T., Mouthereau, F., Lee, C. T., Deramond, J., Lee, J. F., Yu, M. S., & Liew, P. M. (1997). Quaternary transfer faulting in the Taiwan Foothills: evidence from a multisource approach. Tectonophysics, 274(1–3), 61–82.
Dubois, J. (2001). Identification des linéaments dans les images satellitaires par ajustement et suivi de segments. National Library of Canada= Bibliothèque nationale du Canada, Ottawa.
(EGPC), E. G. P. C. (1996). Gulf of Suez oil fields (a comprehensive overview). EGPC. Cairo,, Egypt.
Faure, S. (2000). Analyse des linéaments géophysiques en relation avec les minéralisations en or et métaux de base de l'Abitibi. Projet, 03A.
Gabrielsen, R. H., Braathen, A., Dehls, J., & Roberts, D. (2002). Tectonic lineaments of Norway. Norsk Geologisk Tidsskrift, 82(3), 153–174.

Geomatics, P. C. I. (2015). Geomatica online help. Available Only at Http://Www. Pcigeomatics. Com/Geomatica-Help/(Accessed 08/01/2016).

Ghorab, M. A. (1961). Abnormal stratigraphic features in Ras Gharib oilfield. Dar El-Kitab.

Hammed, M. S. (2002). Geology and structural architecture of southwest Gulf of Suez, with special emphasis on the Precambrian rocks of Gabal el zeit area, Egypt. Department of Geology, Faculty of Science, Cairo University Cairo--Egypt 2002.

Hashim, M., Ahmad, S., Johari, M. A. M., & Pour, A. B. (2013). Automatic lineament extraction in a heavily vegetated region using Landsat Enhanced Thematic Mapper (ETM+) imagery. Advances in Space Research, 51(5), 874–890.

Hempton, M. R. (1987). Constraints on Arabian plate motion and extensional history of the Red Sea. Tectonics, 6(6), 687–705.

Hobbs, W. H. (1923). Earth features and their meaning: an introduction to geology for the student and the general reader. Macmillan.

Horn, B. K. P. (1981). Hill shading and the reflectance map. Proceedings of the IEEE, 69(1), 14–47.

Hung, L. Q., Batelaan, O., & De Smedt, F. (2005). Lineament extraction and analysis, comparison of LANDSAT ETM and ASTER imagery. Case study: Suoimuoi tropical karst catchment, Vietnam. Remote Sensing for Environmental Monitoring, GIS Applications, and Geology V, 5983, 182–193.

Jackson, J. A., White, N. J., Garfunkel, Z., & Anderson, H. (1988). Relations between normal-fault geometry, tilting and vertical motions in extensional terrains: an example from the southern Gulf of Suez. Journal of Structural Geology, 10(2), 155–170.

Jestin, F., Huchon, P., & Gaulier, J. M. (1994). The Somalia plate and the East African Rift System: present-day kinematics. Geophysical Journal International, 116(3), 637–654.

Jia, D., Li, Y., Lin, A., Wang, M., Chen, W., Wu, X., Ren, Z., Zhao, Y., & Luo, L. (2010). Structural model of 2008 Mw 7.9 Wenchuan earthquake in the rejuvenated Longmen Shan thrust belt, China. Tectonophysics, 491(1–4), 174–184.

Jordán, G., Meijninger, B. M. L., Van Hinsbergen, D. J. J., Meulenkamp, J. E., & Van Dijk, P. M. (2005). Extraction of morphotectonic features from DEMs: Development and applications for study areas in Hungary and NW Greece. International Journal of Applied Earth Observation and Geoinformation, 7(3), 163–182.

Jordan, G., & Schott, B. (2005). Application of wavelet analysis to the study of spatial pattern of morphotectonic lineaments in digital terrain models. A case study. Remote Sensing of Environment, 94(1), 31–38.

Lacina, C. (1996). Interprétation structurale des linéaments par traitement d'image satellitaire: cas des sousprovinces d'Abitibi et d'Opatica (Québec). Memory Presented in Faculty of Humanities. University of Sherbrooke Quebec, Canada.

Langridge, R. M., Ries, W. F., Farrier, T., Barth, N. C., Khajavi, N., & De Pascale, G. P. (2014). Developing sub 5-m LiDAR DEMs for forested sections of the Alpine and Hope faults, South Island, New Zealand: Implications for structural interpretations. Journal of Structural Geology, 64, 53–66.

Le Pichon, X., & Francheteau, J. (1978). A plate-tectonic analysis of the Red Sea Gulf of Aden area. Tectonophysics, 46(3–4), 369–406.

Leech, D. P., Treloar, P. J., Lucas, N. S., & Grocott, J. (2003). Landsat TM analysis of fracture patterns: a case study from the Coastal Cordillera of northern Chile. International Journal of Remote Sensing, 24(19), 3709–3726.

Li, N. (2010). Textural and rule-based lithological classification of remote sensing data, and geological mapping in Southwestern Prieska sub-basin, Transvaal Supergroup, South Africa. lmu.

Loissios, D., Tzelepis, N., & Nakos, B. (2021). A methodology for creating analytical hill-shading by combining different lighting directions.

Marghany, M., & Hashim, M. (2010). Lineament mapping using multispectral remote sensing satellite data. International Journal of Physical Sciences, 5(10), 1501–1507.

Mark, R. K. (1992). A multidirectional, oblique-weighted, shaded-relief image of the Island of Hawaii.

Masoud, A., & Koike, K. (2006). Tectonic architecture through Landsat-7 ETM+/SRTM DEM-derived lineaments and relationship to the hydrogeologic setting in Siwa region, NW Egypt. Journal of African Earth Sciences, 45(4–5), 467–477.

McKenzie, D. P., Davies, D., & Molnar, P. (1970). Plate tectonics of the Red Sea and east Africa. Nature, 226(5242), 243–248.

Meshkani, S. A., Mehrabi, B., Yaghubpur, A., & Sadeghi, M. (2013). Recognition of the regional lineaments of Iran: Using geospatial data and their implications for exploration of metallic ore deposits. Ore Geology

Reviews, 55, 48–63.
Meshref, W. M. (2017). Tectonic framework. In The Geology of Egypt (pp. 113–155). Routledge. https://doi.org/10.1201/9780203736678-8
Montenat, C., D'Estevou, P. O., Purser, B., Burollet, P.-F., Jarrige, J.-J., Orszag-Sperber, F., Philobbos, E., Plaziat, J.-C., Prat, P., Richert, J.-P., & others. (1988). Tectonic and sedimentary evolution of the Gulf of Suez and the northwestern Red Sea. Tectonophysics, 153(1–4), 161–177.
Morgan, P. (2017). Egypt in the framework of global tectonics. In The geology of Egypt (pp. 91–111). Routledge.
Morley, C. K. (1995). Developments in the structural geology of rifts over the last decade and their impact on hydrocarbon exploration. Geological Society, London, Special Publications, 80(1), 1–32.
Moustafa, A R, & El-Raey, A. K. (1993). Structural characteristics of the Suez rift margins. Geologische Rundschau, 82(1), 101–109.
Moustafa, Adel R. (n.d.). Explanatory Notes for the Geologic Maps of the Eastern Side of the Suez Rift (Western Sinai Peninsula), Egypt by. 1–34.
Onorati, G., Ventura, R., Poscolieri, M., Chiarini, V., & Crucilla, U. (1992). The digital elevation model of Italy for geomorphology and structural geology. Catena, 19(2), 147–178.
Ott, P., Jarrige, J., & Richert, P. (1998). Chapter 85 Rift development in the Gulf of Suez and the north-western Red Sea : structural aspects and related sedimentary processes.
Owe, M., & de Griend, A. A. (1998). Comparison of soil moisture penetration depths for several bare soils at two microwave frequencies and implications for remote sensing. Water Resources Research, 34(9), 2319–2327.
Paillou, P. (2017). Mapping palaeohydrography in deserts: contribution from space-borne imaging radar. Water, 9(3), 194.
Panizza, M., Castaldini, D., Bollettinari, G., Carton, A., & Mantovani, F. (1987). Neotectonic research in applied geomorphological studies.
Patton, T. L., Moustafa, A. R., Nelson, R. A., & Abdine, S. A. (1994). Tectonic evolution and structural setting of the Suez Rift: Chapter 1: Part I. Type Basin: Gulf of Suez.
Pike, R. J. (1991). Surface features of central North America: A synoptic view from computer graphics. GSA Today, 1(11), 1–251.
Pour, A. B., & Hashim, M. (2014). Structural geology mapping using PALSAR data in the Bau gold mining district, Sarawak, Malaysia. Advances in Space Research, 54(4), 644–654.
Pour, A. B., & Hashim, M. (2015). Structural mapping using PALSAR data in the Central Gold Belt, Peninsular Malaysia. Ore Geology Reviews, 64, 13–22.
Pour, A. B., Hashim, M., Makoundi, C., & Zaw, K. (2016). Structural mapping of the Bentong-Raub suture zone using PALSAR remote sensing data, Peninsular Malaysia: implications for sediment-hosted/orogenic gold mineral systems exploration. Resource Geology, 66(4), 368–385.
Radaideh, O. M. A., Grasemann, B., Melichar, R., & Mosar, J. (2016). which should be cited to refer to this work . Detection and analysis of morphotectonic features utilizing satellite remote sensing and GIS : An example in SW Jordan. Geomorphology, 275, 58–79. https://doi.org/10.1016/j.geomorph.2016.09.033
Ramli, M. F., Yusof, N., Yusoff, M. K., Juahir, H., & Shafri, H. Z. M. (2010). Lineament mapping and its application in landslide hazard assessment: a review. Bulletin of Engineering Geology and the Environment, 69(2), 215–233.
Ranganai, R. T., & Ebinger, C. J. (2008). Aeromagnetic and Landsat TM structural interpretation for identifying regional groundwater exploration targets, south-central Zimbabwe Craton. Journal of Applied Geophysics, 65(2), 73–83.
Saadi, N. M., Zaher, M. A., El-Baz, F., & Watanabe, K. (2011). Integrated remote sensing data utilization for investigating structural and tectonic history of the Ghadames Basin, Libya. International Journal of Applied Earth Observation and Geoinformation, 13(5), 778–791.
Sarp, G. (2005). Lineament analysis from satellite images, north-west of Ankara. Middle East Technical University.
Shake, S. N., & McHone, J. G. (1987). Topographic lineaments and their geologic significance in central New England and adjacent New York. Northeastern Geology, 9(3), 120–128.
Solomon, S., & Ghebreab, W. (2006). Lineament characterization and their tectonic significance using Landsat TM data and field studies in the central highlands of Eritrea. Journal of African Earth Sciences, 46(4), 371–378.
Tchoukanski, I. (2015). EasyCalculate 10, a Set of Expressions for ArcGIS 10. ET Spatial Techniques, Pretoria, South Africa. Available Online at Http://Www. Ian-Ko. Com (Accessed 06/01/2016).

Winn Jr, R. D., Crevello, P. D., & Bosworth, W. (2001). Lower Miocene Nukhul Formation, Gabal el Zeit, Egypt: Model for structural control on early synrift strata and reservoirs, Gulf of Suez. AAPG Bulletin, 85(10), 1871–1890.

Youssef, M. I. (1957). Upper Cretaceous rocks in Quesir area. Bulletin de L'Institute de Egypt, 7, 35–63.

Zaky, K. S. (2017). Paleostress Analysis of the Brittle Deformations on the Northwestern Margin of the Red Sea and the Southern Gulf of Suez , Egypt 1. 51(6), 625–652. https://doi.org/10.1134/S0016852117060097